ACS OMEGA

http://pubs.acs.org/journal/acsodf

Article

# Molecular Dynamics Simulations of the Thermal Decomposition of RDX/HTPB Explosives

Junying Wu,* Jiaojiao Wu, Junjian Li, Yiping Shang, and Lang Chen

Cite This: *ACS Omega* 2023, 8, 18851−18862

Read Online

ACCESS | Metrics & More | Article Recommendations

**ABSTRACT:** The addition of binders to energetic materials is known to complicate the thermal decomposition process of such materials. To assess this effect, the present work studied the thermal decomposition of cyclotrimethylene trinitramine (RDX)/hydroxy-terminated polybutadiene (HTPB) mixtures and of pure RDX over the temperature range of 2000−3500 K by combining the classical reaction and first-principles molecular dynamics methods. The incorporation of HTPB as a binder was found to significantly reduce the decomposition rate of RDX. At 3500 K, the decay rate constant of RDX in the RDX/HTPB system is 2.0141 × $10^{12}$ $s^{-1}$, while it is 2.7723 × $10^{12}$ $s^{-1}$ in the pure RDX system. However, the binder HTPB had little effect on the initial decomposition mechanism, which involved the rupture of N−$NO_2$ bonds to produce $NO_2$. The HTPB was predicted to undergo dehydrogenation and chain breaking. The free H resulting from these processes was predicted to react with low-molecular-weight intermediates generated by the RDX, resulting in greater equilibrium quantities of the final products $H_2O$ and $H_2$ being obtained from the mixed system compared with pure RDX. HTPB-chain fragments were also found to combine with the primary RDX decomposition product $NO_2$ to inhibit the formation of $N_2$ and $CO_2$.

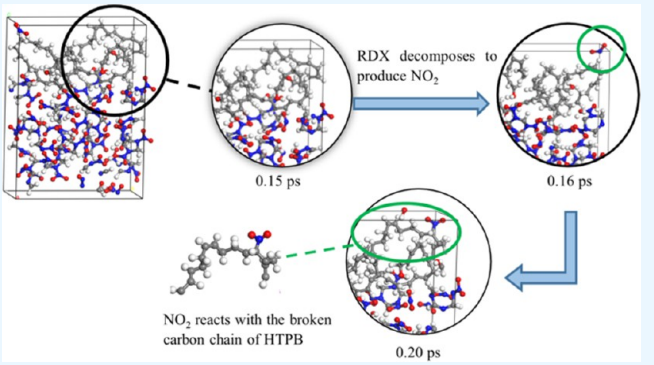


## 1. INTRODUCTION

Cyclotrimethylene trinitramine (RDX) is a high-energy nitramine explosive that exhibits exceptional detonation performance and has many military and civilian applications.[1,2] Even so, explosives based solely on RDX have several shortcomings, such as poor safety performance and difficulty in forming. For these reasons, binders are often added to reduce the sensitivity of the explosive while also improving the molding and mechanical properties. Unfortunately, the thermal decomposition mechanisms associated with these multi-component explosives are more complex. Specifically, the intermediate and final products generated during thermal decomposition may oxidize the polymeric binders in mixed explosives, thus affecting the detonation performance. Consequently, further study of the thermal decomposition behaviors, reaction mechanisms, and sensitivities of these materials is required. Even so, the thermal decomposition of explosives is extremely rapid and so it is often difficult to assess the associated reactions in detail experimentally. Molecular dynamics simulation offers an alternative approach to elucidating the thermal decomposition mechanisms of high explosives on the atomic level. In this regard, first-principles and classical reaction molecular dynamics are especially helpful.[3−6]

In terms of classical reactive molecular dynamics research, Strachan et al.[7] first used reactive molecular dynamics calculations based on the ReaxFF force field to simulate the thermal decomposition of RDX at different temperatures and densities in 2005. This prior work indicated that the cleavage of N−N bonds to generate $NO_2$ is the primary reaction during the early stage of thermal decomposition. The production of CO and $CO_2$ was also found to be largely determined by density. At low and high densities, CO and $CO_2$ were shown to be the main products, respectively, although density evidently had little effect on the production of $N_2$ and $H_2O$. In 2017, Peng et al.[8] also used ReaxFF reaction molecular dynamics method to study the thermal decomposition mechanism of RDX and its derivatives at high temperature. The results showed that the first step of RDX pyrolysis was the cleavage of the N−$NO_2$ bonds to generate $NO_2$, followed by the loss of side chains or ring opening. The intermediates $NO_2$ and NO

Received: February 20, 2023
Accepted: April 28, 2023
Published: May 16, 2023

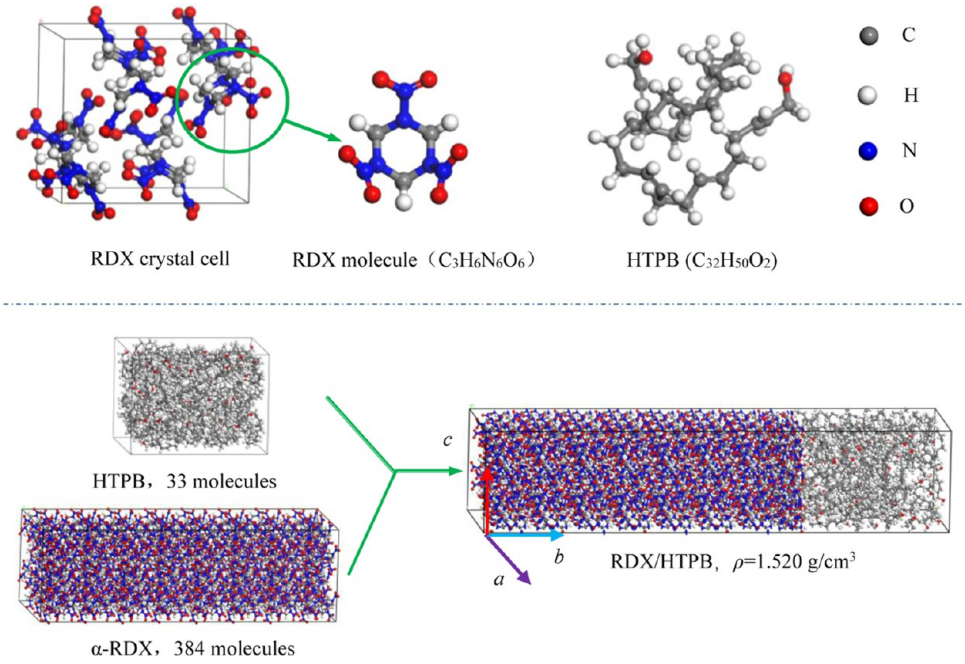


**Figure 1.** Classical reaction molecular dynamics model of the RDX/HTPB system.

were also determined to undergo secondary reactions to form $N_2$ such that the end products were $N_2$, $H_2O$, and $CO_2$. The molecular dynamics of the thermal decomposition of RDX have been extensively studied but, because RDX is commonly used in mixed explosives, simulations of the thermal decomposition of such mixtures would be more valuable with regard to practical applications.[9−12] In 2006, Zhang[13] used the ReaxFF reaction molecular dynamics method to compare the thermal decomposition characteristics of RDX with and without a polyurethane binder. The results showed that the addition of the binder significantly reduced the thermal decomposition rate of RDX, although the products of decomposition were basically the same.

First-principles molecular dynamics calculations can accurately describe chemical reactions, while the density functional tight binding (DFTB) method improves the calculation speed and is widely used in the study of the thermal decomposition mechanism of explosives.[14,15] In 2002, Manaa et al.[16] used first-principles molecular dynamics calculations based on the self-consistent charge density functional tight binding method (SCC-DFTB) to model the reaction of octahydro-1,3,5,7-tetranitro-1,3,5,7-tetrazocine (HMX) at 3500 K and predicted the rates of formation of typical products such as $H_2O$, $CO_2$, and $N_2$. In 2019, He et al.[17] studied the electronic properties and thermal decomposition behavior of an HMX/hydroxy-terminated polybutadiene (HTPB) plastic-bonded explosive using the first-principles molecular dynamics method based on SCC-DFTB. The results showed that the electrostatic interaction between the nitro group oxygen atoms of the HMX and hydroxyl butyrate groups of the HTPB significantly stabilized the surfaces of the HMX crystals. The incorporation of HTPB therefore inhibited the thermal decomposition of the HMX. The HTPB binder was also found to be highly stable such that the majority of polymer chains were predicted to remain intact following the reaction.

Currently, classical reaction molecular dynamics and first-principles molecular dynamics methods have been widely used to investigate the initial reaction paths and product formation of RDX and other explosives, which have provided a detailed understanding of their thermal decomposition mechanism. However, most explosives used in practice are mixed materials, and there is a lack of research on their thermal decomposition mechanism. Furthermore, there is a deficiency in a systematic analysis of the possible reactions that may occur between explosives and adhesives and their impact on the resulting products. Therefore, further research on the thermal decomposition mechanism of mixed explosives is necessary to ensure their safe use and promote their development.

On this basis, the present study employed the classical reaction molecular dynamics method based on the ReaxFF-lg reaction force field and the first-principles molecular dynamics method in conjunction with SCC-DFTB theory to simulate the thermal decomposition of RDX/HTPB explosives at high temperatures. The thermal decomposition characteristics of pure RDX and of RDX/HTPB were assessed at 3500, 3000, 2500, and 2000 K using classical reaction molecular dynamics, while the thermal decomposition of RDX/HTPB at 3000 K was modeled based on first-principles molecular dynamics. In this manner, the effect of HTPB on the decomposition of RDX was examined.

## 2. COMPUTATIONAL MODELS AND METHODS

**2.1. Construction of Computational Models.** The properties of $\alpha$-RDX are the most stable at room temperature, and the crystal structure of this compound ($a$ = 11.443 Å, $b$ = 10.611 Å, $c$ = 13.156 Å, $\alpha = \beta = \gamma = 90°$) has been determined based on X-ray diffraction data.[18] HTPB is a homopolymer containing cis-1,4, trans-1,4, and trans-1,2 double bonds and, in the present work, was assumed to be based on a trans-1,4 monomer. In this model, the terminal groups were saturated with −H to construct a single-chain structure with $n$ = 8 having the molecular formula $C_{32}H_{50}O_2$. Figure 1 shows the classical reaction molecular dynamics model derived for RDX/HTPB. This model was generated by first using the Material Studio (MS) program to construct a 3 × 2 × 2 supercell structure based on the RDX cell, after which a 5 ps temperature and


https://doi.org/10.1021/acsomega.3c01160
ACS Omega 2023, 8, 18851−18862

pressure relaxation was performed under regular ensemble NVT and constant temperature and pressure ensemble NPT conditions, respectively, to obtain a stable structure at 300 K and 0 GPa. This stable structure was subsequently expanded four times along the *b* direction. The PACKMOL program[19] was then used to place 33 HTPB chains into a box of appropriate size to produce an HTPB system having a reasonable stacking mode via optimization calculations. Following this, the 10 and 50 ps relaxations were performed under NVT and NPT ensemble conditions, respectively. The resulting HTPB system was placed 10 Å away from the RDX supercell along the *b* direction of the supercell in the MS and then compressed at a specific speed along this same direction until there was no significant gap between the two systems and no mutual extrusion. Finally, the RDX/HTPB hybrid system was optimized at a temperature of 300 K to build a computational system having a reasonable density.

Figure 2 provides the first-principles molecular dynamics calculation model employed for the RDX/HTPB analysis.

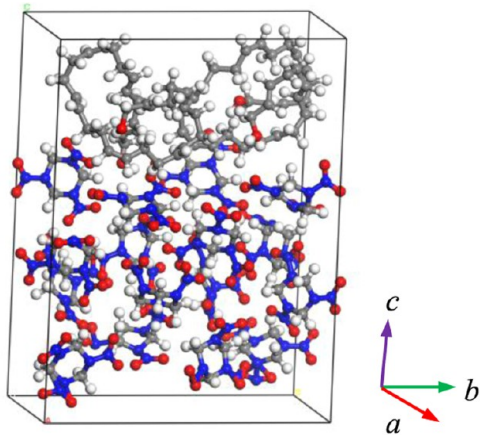


**Figure 2.** First-principles molecular dynamics model of the RDX/HTPB system.

Based on the computing power required for this method, a 1 × 2 × 1 cell expansion was performed along the *a*, *b*, and *c* directions of an RDX single cell to obtain a supercell containing 16 RDX molecules (equivalent to 336 atoms). Two HTPB chains with a number of 8 were subsequently added along the [001] crystal plane. The conjugate gradient (CG) method in the CP2K package[20] was used to optimize the cell parameters and conformation of the RDX/HTPB model so as to obtain a stable structure based on the DFTB process. The convergence criteria comprised a maximum geometric displacement near 20,000 steps of less than 0.003 b, a root mean square of less than 0.0015 b, a force component change of less than 0.00045 hartree/b, and a maximum root-mean-square force of less than 0.0003 hartree/b. Using these criteria in conjunction with a temperature and pressure of 300 K and 0 GPa, the RDX/HTPB model was calculated for 2 ps under NVT and NPT ensemble conditions, respectively, with a time step of 0.2 fs so as to further optimize the internal stress and allow the system to reach equilibrium. The equilibrium parameters determined for the RDX/HTPB system were $a$ = 10.756 Å, $b$ = 20.674 Å, $c$ = 28.047 Å, $\alpha = 90°$, $\beta = 90°$, and $\gamma = 90°$.

**2.2. Computational Methods and Parameters.** *2.2.1. Classical Molecular Dynamics Method.* The force field is a function used in classical molecular dynamics simulations to describe intermolecular forces and can determine the accuracy of the calculation results. With the development of various applications for molecular dynamics, these functions have become increasingly complex. Traditional molecular dynamics methods are able to model the evolution of a system over time but cannot simulate bond cleavage and so are unable to model chemical reactions. For this reason, force field functions capable of describing chemical reactions have been developed, including the ReaxFF function based on the theory of bond order as proposed by van Duin et al.[21] in 2001. This method has been widely used to simulate the chemical reactions of explosives. In these simulations, the breaking and forming of chemical bonds are determined by the bond lengths between atoms and the parameters of the force field function are fitted according to the results of first-principles calculations, such that the ReaxFF force field can provide approximately the same level of accuracy as quantum mechanics. In addition, the calculation costs associated with the force field method are low and so calculations involving millions of atoms are possible. The long-range interactions between molecules were subsequently incorporated into the ReaxFF function by adding dispersion forces to give the improved ReaxFF-lg force field function. The latter is able to describe crystal structures more accurately and so was used in the present work to simulate the chemical reactions of RDX/HTPB mixtures at high temperatures. Because research by Liu et al.[22] has confirmed that the predicted RDX structures obtained using the ReaxFF-lg force field approach are generally consistent with experimental data, this paper assumes that this method is applicable to the analysis of RDX.

To verify the applicability of the ReaxFF-lg force field function to modeling of the HTPB binder, the radial distribution function, $g(r)$, for HTPB following relaxation was determined and compared with the literature value. Figure 3 shows the radial distribution function obtained for HTPB after relaxation, while Table 1 compares the peak positions in this calculated function with the literature values. It can be seen from these results that the radial distribution function predicted using the ReaxFF-lg method was consistent with the literature data. This agreement indicates that the ReaxFF-lg

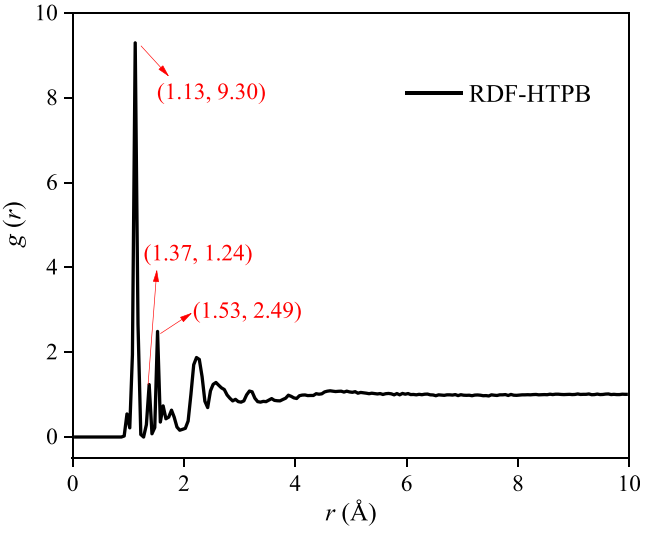


**Figure 3.** Radial distribution function determined for HTPB at 300 K.



https://doi.org/10.1021/acsomega.3c01160
ACS Omega 2023, 8, 18851−18862

**Table 1. Comparison of the Peak Positions in the Calculated HTPB Radial Distribution Function with Reference Values**

| HTPB | C−H (Å) | C═C (Å) | C−C (Å) |
|---|---|---|---|
| reference[23] | 1.13 | 1.37 | 1.53 |
| ReaxFF-lg | 0.96 | 1.35 | 1.52 |

force field is a suitable means of performing molecular dynamics calculations for HTPB.

The classical reaction molecular dynamics calculations were carried out using the large-scale atomic/molecular massively parallel simulator (LAMMPS) program. After obtaining the equilibrium structure for the RDX/HTPB and RDX systems, the NVE microcanonical ensemble and Berendsen thermal bath processes were employed to rapidly increase the temperature of each system to 2000, 2500, 3000, or 3500 K after which the resulting chemical reactions were analyzed using a time step of 0.1 fs. The cleavage of bonds during the chemical reactions was assessed by setting the cutoff radius of atomic pair bond orders to 0.3.[24]

*2.2.2. First-Principles Molecular Dynamics Methods.* Because the results of classical molecular dynamics simulations are greatly affected by the force field used, the accuracy obtained from such calculations is lower than that from first-principles molecular dynamics methods based on the Schrödinger equation or density functional theory (DFT). In the work reported herein, the CP2K first-principles molecular dynamics software package was used to calculate the thermal decomposition behavior of the RDX/HTPB system at high temperatures. CP2K is an ab initio molecular dynamics simulation package that was first developed by the Max Planck Research Center in Germany in 2000. This software is primarily used to calculate the atomic and molecular dynamics of solids, liquids, macromolecules, crystals, and biological systems. In the case of the present calculations, the interatomic forces were determined using the SCC-DFTB method, which is a tight binding approach based on the DFT. This method is able to accurately estimate the molecular structures associated with specific periodic boundary conditions and to describe the chemical bond reactions and weak interaction between molecules.

During the present first-principles molecular dynamics calculations, the RDX/HTPB system was rapidly heated to 3000 K using a Nose−Hoover thermal bath in NVT ensemble conditions. The self-consistent convergence accuracy was set to $10^{-5}$ au, the integration time step was 0.2 fs, and the total computation time was 5 ps. The molecular movement track was recorded at 0.2 fs intervals to allow a subsequent analysis of the reaction mechanism, associated species, and bond-breaking statistics. The atomic positions at each time interval were processed to obtain snapshots, species information, and bond-level files.

## 3. RESULTS AND DISCUSSION

**3.1. Evolution of Potential Energy and Number of Species.** Using the classical molecular dynamics method, the potential energy values for the RDX/HTPB system over time at different temperatures were obtained and are plotted in Figure 4. These data demonstrate that, at all temperatures, the potential energy rapidly increased to a peak value in a very short time, and the higher the temperature is, the higher the peak value of potential energy is, and the maximum value of

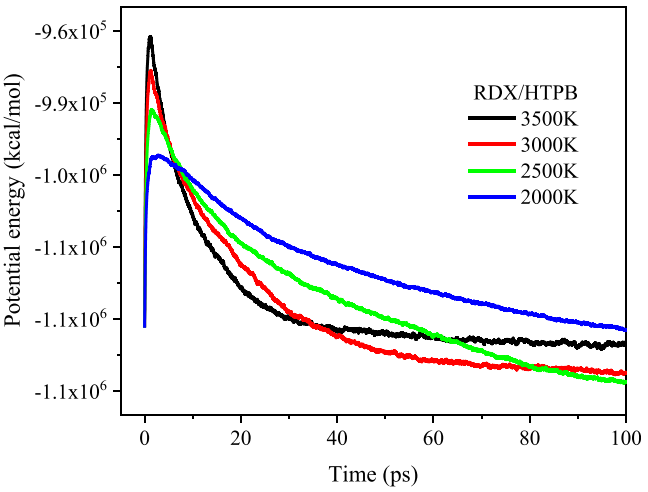


**Figure 4.** Potential energy values for the RDX/HTPB system at various temperatures as functions of time.

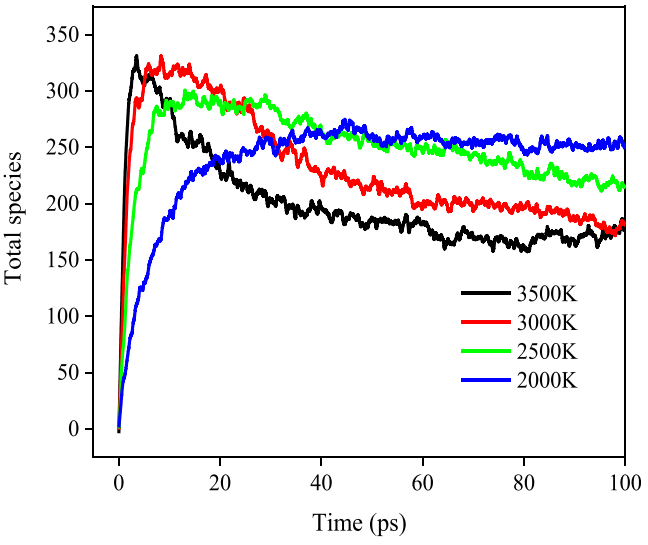


**Figure 5.** Total species values for the RDX/HTPB system at various temperatures as functions of time.

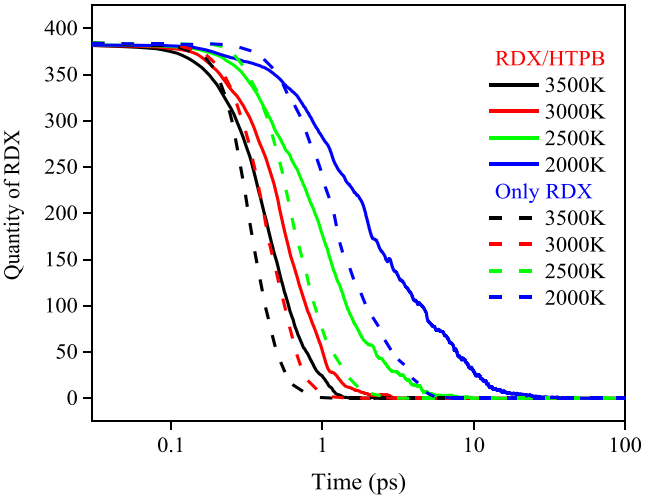


**Figure 6.** Quantities of RDX molecules for two systems as functions of time in RDX/HTPB and pure RDX systems.



https://doi.org/10.1021/acsomega.3c01160
ACS Omega 2023, 8, 18851−18862

**Table 2. Rate Constants for RDX Decay in RDX/HTPB and Pure RDX Systems at Different Temperatures**

| system | temperature (K) | decay rate $k$ ($10^{12}$ $s^{-1}$) |
|---|---|---|
| RDX/HTPB | 2000 | 0.2813 |
| | 2500 | 0.8230 |
| | 3000 | 1.5619 |
| | 3500 | 2.0141 |
| only RDX | 2000 | 0.6222 |
| | 2500 | 1.3147 |
| | 3000 | 2.1260 |
| | 3500 | 2.7723 |

potential energy is reached at 3500 K. Subsequently, the potential energy decreased rapidly and then more slowly to produce an equilibrium in the late stage of the reaction. The shape of these plots can be attributed to the rapid absorption of heat from the reaction and the primary decomposition reaction in the early stage, which increased the potential energy. With the accumulation of heat, secondary thermal decomposition reactions began to occur in the system to generate a large number of intermediate and final products along with significant heat. The potential energy of the system thus decreased rapidly and finally produced an equilibrium. In the case of the RDX/HTPB system, the time spans required for the potential energy to reach the maximum value at 3500, 3000, 2500, and 2000 K were determined to be 1.16, 1.22, 1.4, and 1.62 ps, respectively. Thus, higher temperatures were associated with shorter time intervals. That is, a higher temperature caused the potential energy to decrease more rapidly and so shortened the time required to reach equilibrium.

Figure 5 plots the number of species for the RDX/HTPB system over time at different temperatures. It is evident that, at the beginning of the reaction, the system contained two kinds of molecules. However, as the thermal decomposition reactions progressed, the number of molecules in the system increased rapidly to a maximum, after which secondary reactions consumed many of the small molecules and the number of species began to decline. Eventually, a dynamic equilibrium was achieved. The RDX/HTPB system exhibited the maximum number of species at 3.52, 8.36, 13.09, and 44.66 ps for temperatures of 3500, 3000, 2500, and 2000 K, respectively. Therefore, as expected, higher temperatures produced faster reaction rates. Note also that, at a relatively low temperature of 2000 K, fewer secondary reactions would be expected and so the number of species did not exhibit a downward trend after reaching the peak. Both the potential energy and species number data sets also indicate that the thermal decomposition reactions of the RDX/HTPB system were essentially complete by 100 ps.

### 3.2. Decay Rate of RDX Molecules in a Mixed System.

Analyzing the results obtained from the classical reaction

**Table 3. Parameters for the Single-Molecule Decomposition Reaction of RDX in the RDX/HTPB System at Different Temperatures**

| $T$ (K) | frequencies | reaction time (ps) | primary reaction |
|---|---|---|---|
| 3500 | 592 | 0.03−1.6 | $C_3H_6N_6O_6 \rightarrow NO_2 + C_3H_6N_5O_4$ |
| | 9 | 0.2−1.23 | $C_3H_6N_6O_6 \rightarrow 2NO_2 + C_3H_6N_4O_2$ |
| | 7 | 0.34−1.28 | $C_3H_6N_6O_6 \rightarrow HNO_2 + C_3H_5N_5O_4$ |
| | 3 | 0.38−0.49 | $C_3H_6N_6O_6 \rightarrow O + C_3H_6N_6O_5$ |
| | 9 | 0.63−2.16 | $C_3H_6N_6O_6 \rightarrow NO_3 + C_3H_6N_5O_3$ |
| | 2 | 0.69−0.75 | $C_3H_6N_6O_6 \rightarrow NO_2 + HNO_2 + C_3H_5N_4O_2$ |
| | 2 | 1.21−2.11 | $C_3H_6N_6O_6 \rightarrow N_2O_5 + C_3H_6N_4O$ |
| | 2 | 1.26−1.47 | $C_3H_6N_6O_6 \rightarrow NO + C_3H_6N_5O_5$ |
| | 5 | 1.78−2.03 | $C_3H_6N_6O_6 \rightarrow N_2O_4 + C_3H_6N_4O_2$ |
| 3000 | 633 | 0.02−2.8 | $C_3H_6N_6O_6 \rightarrow NO_2 + C_3H_6N_5O_4$ |
| | 3 | 0.2−0.36 | $C_3H_6N_6O_6 \rightarrow O + C_3H_6N_6O_5$ |
| | 8 | 0.46−2.04 | $C_3H_6N_6O_6 \rightarrow 2NO_2 + C_3H_6N_4O_2$ |
| | 13 | 0.55−2.7 | $C_3H_6N_6O_6 \rightarrow NO_3 + C_3H_6N_5O_3$ |
| | 2 | 0.64−3.02 | $C_3H_6N_6O_6 \rightarrow NO_2 + HO + C_3H_5N_5O_3$ |
| | 2 | 0.69−1.57 | $C_3H_6N_6O_6 \rightarrow NO_2 + HNO_2 + C_3H_5N_4O_2$ |
| | 9 | 0.72−1.52 | $C_3H_6N_6O_6 \rightarrow HNO_2 + C_3H_5N_5O_4$ |
| | 3 | 1.4−4.26 | $C_3H_6N_6O_6 \rightarrow HNO_3 + C_3H_5N_5O_3$ |
| 2500 | 807 | 0.08−7.75 | $C_3H_6N_6O_6 \rightarrow NO_2 + C_3H_6N_5O_4$ |
| | 18 | 0.38−7.22 | $C_3H_6N_6O_6 \rightarrow HNO_2 + C_3H_5N_5O_4$ |
| | 9 | 0.52−3.39 | $C_3H_6N_6O_6 \rightarrow NO_3 + C_3H_6N_5O_3$ |
| | 5 | 0.88−3.85 | $C_3H_6N_6O_6 \rightarrow 2NO_2 + C_3H_6N_4O_2$ |
| | 2 | 1.05−1.27 | $C_3H_6N_6O_6 \rightarrow CH_2N_2O_2 + C_2H_4N_4O_4$ |
| | 2 | 4.04−6.87 | $C_3H_6N_6O_6 \rightarrow HNO_3 + C_3H_5N_5O_3$ |
| 2000 | 867 | 0.11−9.95 | $C_3H_6N_6O_6 \rightarrow NO_2 + C_3H_6N_5O_4$ |
| | 4 | 0.63−3.78 | $C_3H_6N_6O_6 \rightarrow 2NO_2 + C_3H_6N_4O_2$ |
| | 11 | 0.76−8.32 | $C_3H_6N_6O_6 \rightarrow NO_3 + C_3H_6N_5O_3$ |
| | 2 | 2.03−2.36 | $C_3H_6N_6O_6 \rightarrow NO_2 + HNO_2 + C_3H_5N_4O_2$ |
| | 20 | 2.7−9.95 | $C_3H_6N_6O_6 \rightarrow N_2O_4 + C_3H_6N_4O_2$ |
| | 6 | 3.15−9.09 | $C_3H_6N_6O_6 \rightarrow HN_2O_4 + C_3H_5N_4O_2$ |
| | 13 | 3.45−9.77 | $C_3H_6N_6O_6 \rightarrow HNO_2 + C_3H_5N_5O_4$ |
| | 2 | 9.13−9.84 | $C_3H_6N_6O_6 \rightarrow HNO_3 + C_3H_5N_5O_3$ |



https://doi.org/10.1021/acsomega.3c01160
ACS Omega 2023, 8, 18851−18862

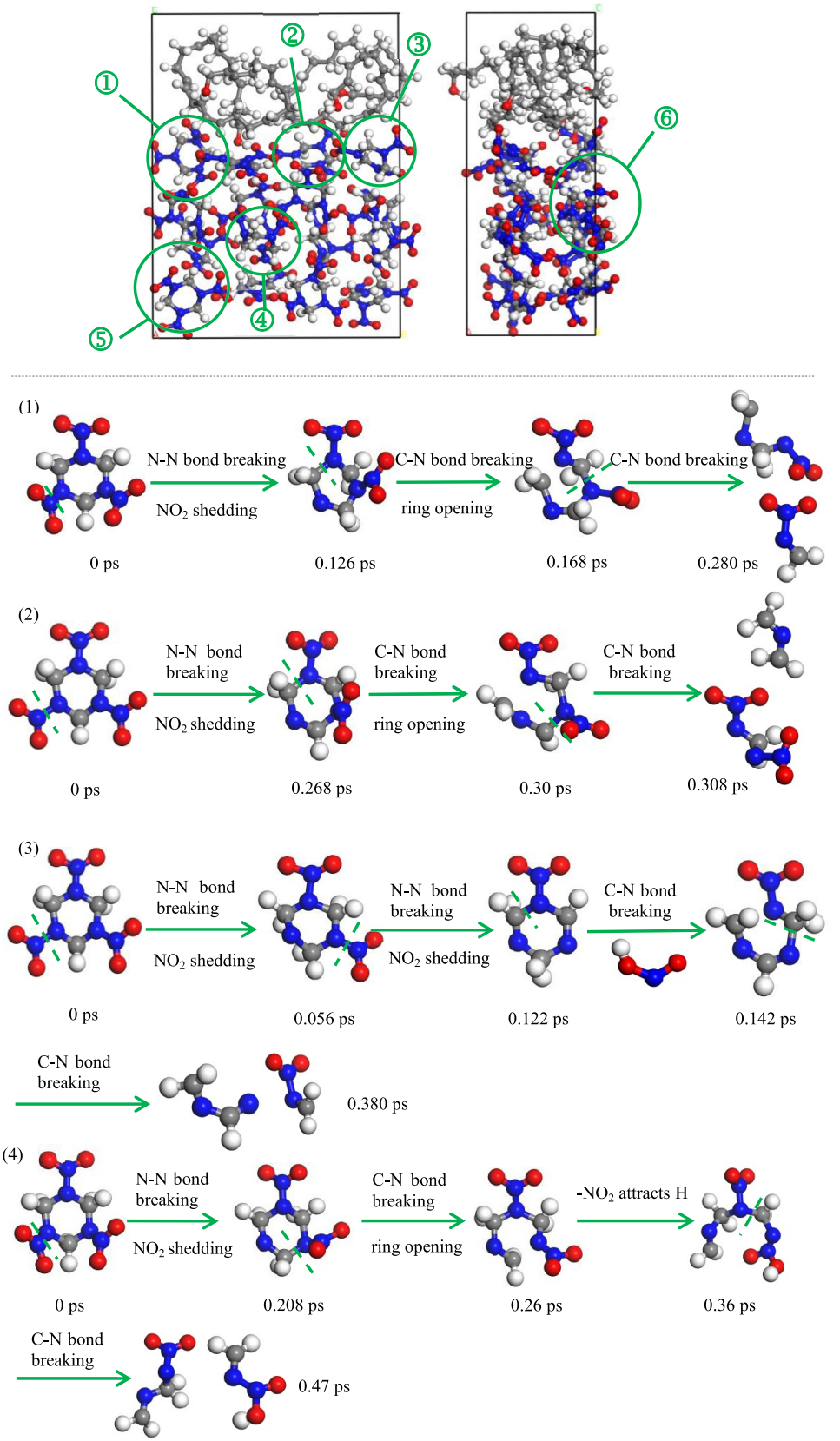


**Figure 7.** continued



https://doi.org/10.1021/acsomega.3c01160
*ACS Omega* 2023, 8, 18851−18862

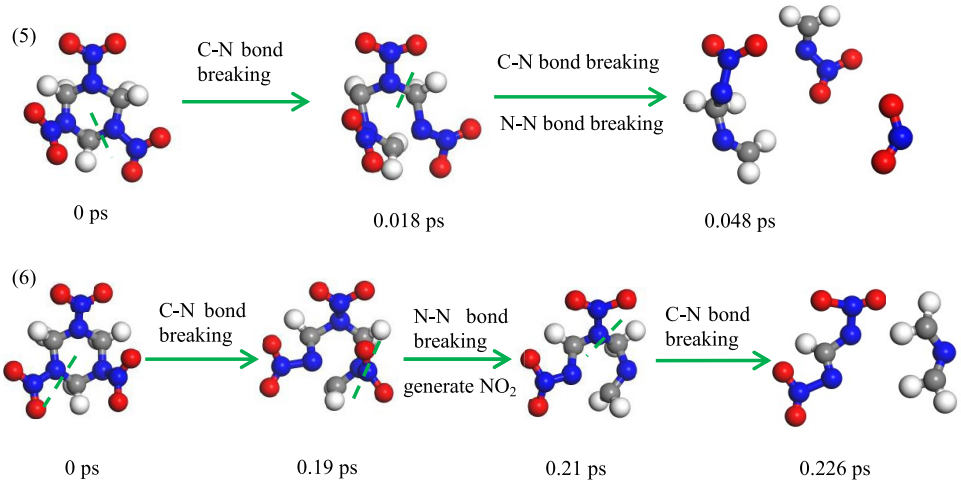


**Figure 7.** Six possible pathways for the decomposition of RDX in the RDX/HTPB system.

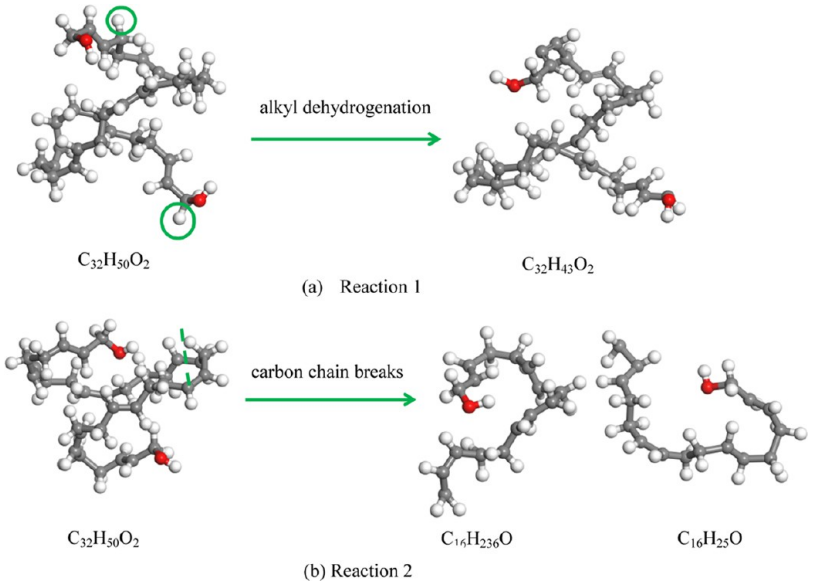


**Figure 8.** Decomposition reactions of HTPB molecules.

molecular dynamics calculations provided data regarding the RDX quantities over time in the RDX/HTPB and RDX systems at different temperatures, as shown in Figure 6. The number of RDX molecules in both systems can be seen to have decreased rapidly after the reaction started, with more rapid decomposition at higher temperatures and complete decomposition within 100 ps. In the case of the RDX/HTPB system, the time intervals required for the complete decomposition of the RDX at 3500, 3000, 2500, and 2000 K were found to be 1.41, 2.95, 9.59, and 35.95 ps, respectively. These data also indicate that the decomposition of RDX in RDX/HTPB would be expected to occur more slowly than that of pure RDX at all temperatures.

The decay of nitramine explosives during thermal decomposition can be summarized by the equation

$$C(t) = C_0 \exp(-kt) \quad (1)$$

where $C_0$ is the initial number of RDX molecules, $C(t)$ is the number of RDX molecules at time $t$, and $k$ is the decay rate constant ($10^{12}$ $s^{-1}$). The data in Figure 6 for the RDX/HTPB and pure RDX systems were fit using this equation, and the resulting values for $k$ are summarized in Table 2. It is apparent from these results that the value of $k$ increased along with the temperature. In addition, for a given temperature, the extent to which the RDX in the RDX/HTPB system decomposed was significantly lower than that in the pure RDX. These results confirm that the addition of a relatively small amount of HTPB to RDX as a binder would be expected to reduce the decomposition rate of the explosive.

**3.3. Decomposition Pathways of RDX Molecules in a Mixed System.** Studying the initial decomposition of an energetic material can provide an improved understanding of the reaction mechanism. In the present work, the initial decomposition reaction path of RDX molecules in the RDX/HTPB system at high temperatures was assessed. The bond order files for the first 10 ps of classical reaction molecular dynamics calculations were counted, and all RDX reactions with a reaction frequency of greater than 2 were analyzed. Table 3 provides the initial decomposition reactions and reaction durations for RDX molecules in the RDX/HTPB system at various temperatures.



https://doi.org/10.1021/acsomega.3c01160
ACS Omega 2023, 8, 18851−18862

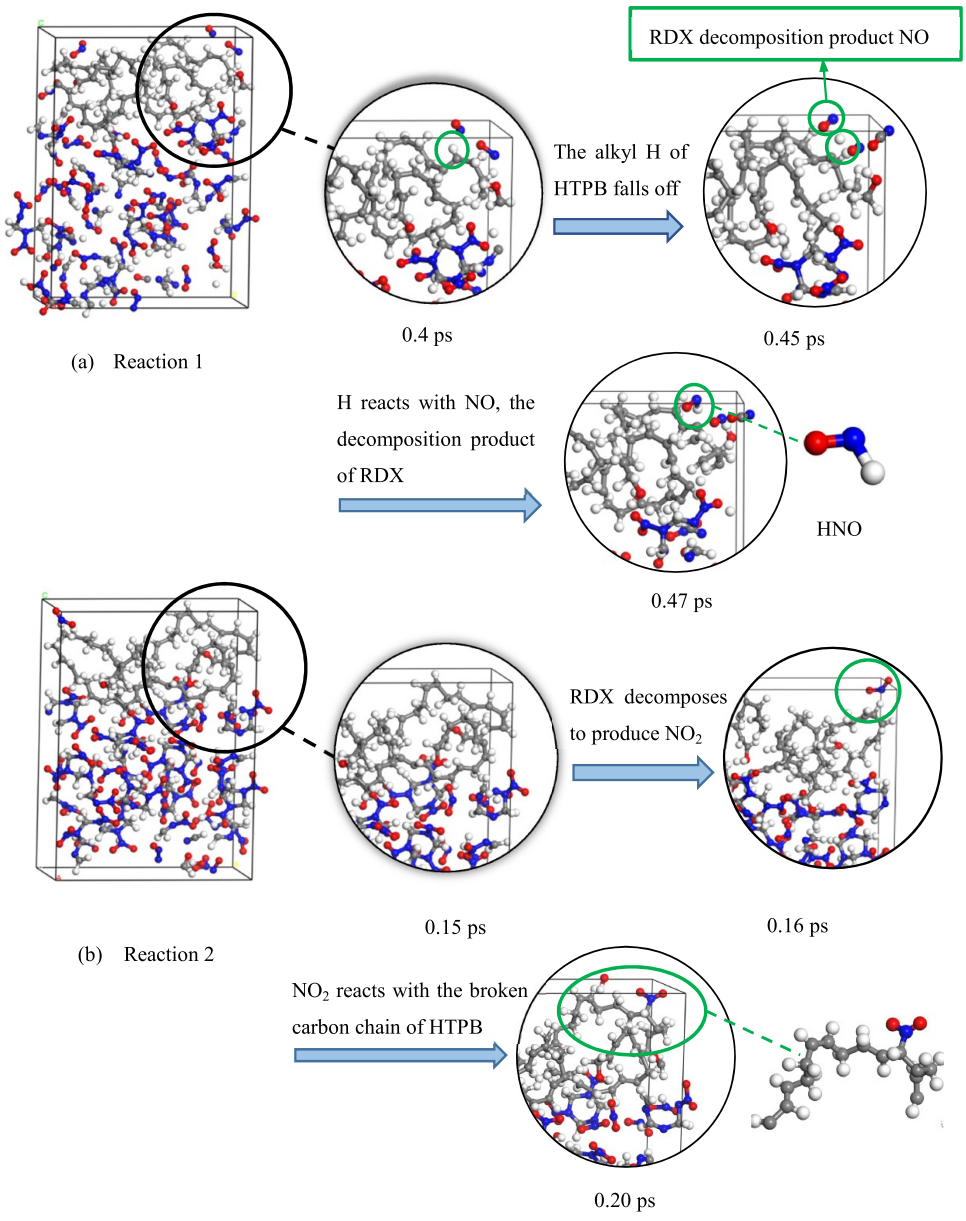


**Figure 9.** Reactions between RDX and HTPB.

It can be seen from Table 3 that four single-molecule decomposition reaction pathways were determined for RDX in RDX/HTPB at high temperatures. These were

$$C_3H_6N_6O_6 \rightarrow NO_2 + C_3H_6N_5O_4 \quad (2)$$

$$C_3H_6N_6O_6 \rightarrow 2NO_2 + C_3H_6N_4O_2 \quad (3)$$

$$C_3H_6N_6O_6 \rightarrow NO_3 + C_3H_6N_5O_3 \quad (4)$$

$$C_3H_6N_6O_6 \rightarrow HNO_2 + C_3H_5N_5O_4 \quad (5)$$

For all four temperatures, the cleavage of the N−$NO_2$ bond to generate $NO_2$ (that is, reaction 2) was found to occur as the first step of decomposition and with the highest frequency. However, higher temperatures were determined to reduce the frequency of this reaction. This trend is attributed to the greater frequency of collisions between molecules at higher temperatures that, in turn, increases the number of multi-molecule polymerization reactions and decreases the frequency of monomolecular decomposition reactions. In reaction 3, both N−$NO_2$ bonds in the RDX ring are broken. Reaction 4 indicates that each nitro group can interact with the oxygen atom on an adjacent nitro group. Reaction 5 represents the transfer of a hydrogen from the RDX ring to the nitro group after which the N−NOHO bond breaks to form $HNO_2$. At 3500 K, the frequency of these four monomolecular decomposition reactions decreased in the order of (2) > (3) = (4) > (5), meaning that the hydrogen transfer reaction was the least likely to occur. At 3000 K, the order was (2) > (4) > (5) > (3) such that the removal of two $NO_2$ molecules was less likely than the hydrogen transfer reaction. At 2500 K, the order was (2) > (5) > (4) > (3). Again, the frequency of the hydrogen transfer reaction was greater than that of the reaction removing two $NO_2$. At 2000 K, the order was (2) > (5) > (4) > (3) although the reaction $C_3H_6N_6O_6 \rightarrow N_2O_4 + C_3H_6N_4O_2$ was also relatively likely to occur. Thus, a lower temperature would be expected to increase the probability of the N−$NO_2$ bond breaking after hydrogen transfer while reducing the rate at which two N−$NO_2$ bonds are broken simultaneously.



https://doi.org/10.1021/acsomega.3c01160
ACS Omega 2023, 8, 18851−18862

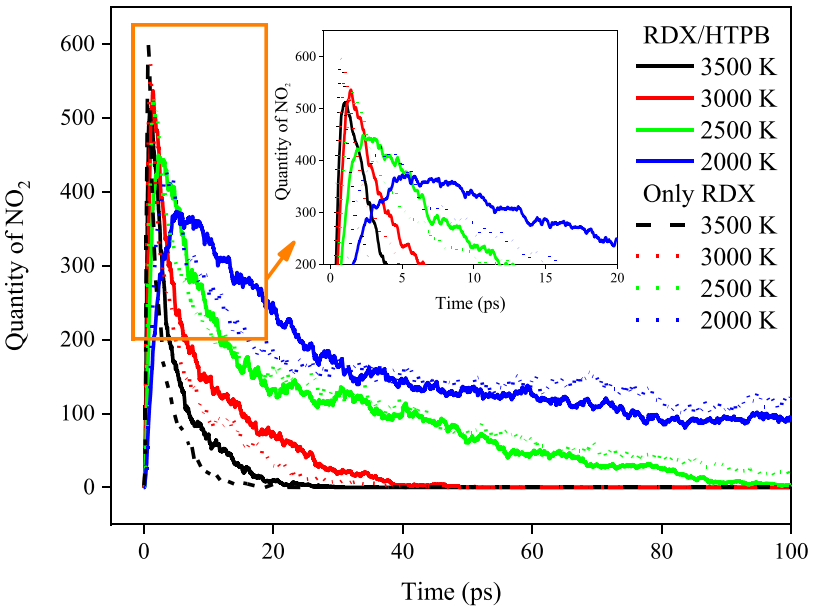


**Figure 10.** Quantity of the primary product $NO_2$ as a function of time for the RDX/HTPB and pure RDX systems at various temperatures.

The initial decomposition mechanism for RDX in the RDX/HTPB system was obtained by analyzing the results of calculations based on classical reaction molecular dynamics. More details were obtained by assessing a total of six decomposition pathways by processing the results of first-principles molecular dynamics calculations, as shown in Figure 7. In the first path, taking the RDX molecule labeled ① as an example, the initial thermal decomposition pathway involves breaking of a N−$NO_2$ bond of the molecule at 0.126 ps with the simultaneous generation of $NO_2$ and is very rapid. Subsequently, at 0.168 ps, a C−N bond breaks and a ring opening reaction occurs. Finally, at 0.28 ps, the C−N bond nearest to a remaining $NO_2$ breaks to provide two intermediate products: $CH_2N_2O_2$ and $C_2H_4N_3O_2$. The reactions involved in this mechanism are therefore

$$C_3H_6N_6O_6 \rightarrow C_3H_6N_5O_4 + NO_2 \quad (6)$$

$$C_3H_6N_5O_4 \rightarrow CH_2N_2O_2 + C_2H_4N_3O_2 \quad (7)$$

In the second decomposition pathway, taking the RDX molecule labeled ② as an example, a N−$NO_2$ bond breaks at 0.268 ps to generate $NO_2$. At 0.30 ps, a C−N bond ruptures and ring opening occurs, after which a second C−N bond breaks at 0.308 ps. Note that this bond is at a different site from the C−N bond-breaking position in the first path. This process generates the intermediate products $C_2H_4N$ and $CH_2N_4O_4$ and can be expressed as

$$C_3H_6N_5O_4 \rightarrow C_2H_4N + CH_2N_4O_4 \quad (8)$$

Using the RDX molecule labeled as ③ to represent the third decomposition pathway, the first step is the cleavage of the N−$NO_2$ bond at 0.056 ps to generate $NO_2$. At 0.122 ps, a second N−$NO_2$ bond breaks to again produce $NO_2$. Following this, a C−N bond breaks and ring opening occurs at 0.142 ps. In addition, a H atom is lost from an alkyl group and reacts with a $NO_2$ to generate $HNO_2$. At 0.380 ps, a second C−N bond ruptures to produce two intermediate products: $C_2H_3N_2$ and $CH_2N_2O_2$. This reaction path is relatively complex but can be summarized as

$$C_3H_6N_6O_6 \rightarrow C_3H_6N_5O_4 + NO_2 \quad (9)$$

$$C_3H_6N_5O_4 + NO_2 \rightarrow C_3H_5N_5O_4 + HNO_2 \quad (10)$$

$$C_3H_5N_5O_4 \rightarrow C_2H_3N_2 + CH_2N_2O_2 \quad (11)$$

In the fourth decomposition pathway involving RDX molecule ④, a N−$NO_2$ bond breaks at 0.208 ps to generate $NO_2$ after which, at 0.260 ps, a C−N bond breaks and the ring opens. At this point, a −$NO_2$ group combines with a H atom generated by another RDX molecule. The fifth decomposition path involving RDX molecule ⑤ begins with the rupture of a C−N bond to open the ring at 0.018 ps, followed by the breaking of a N−N bond and another C−N bond almost simultaneously at 0.048 ps, generating $C_2H_4N_3O_2$, $CH_2N_2O_2$, and $NO_2$. In the sixth decomposition pathway, taking RDX molecule ⑥ as an example, a C−N bond breaks to open the ring at 0.19 ps, after which a N−N bond breaks to generate $NO_2$ at 0.21 ps. A second C−N bond ruptures at 0.226 ps to produce $C_2H_4N$ and $CH_2N_3O_4$.

The monomolecular decomposition pathways obtained from the initial molecular dynamics calculations indicate that the majority of RDX molecules would be expected to first undergo N−$NO_2$ bond breaking followed by the cleavage of a C−N bond to produce ring opening and the breaking of a second N−$NO_2$ bond. The latter two processes compete with one another. Following ring opening, a H atom either from the same molecule or another molecule will be attracted by a remaining −$NO_2$ group. It is also evident that, in some cases, the process will begin with the cleavage of a C−N bond after which a N−N bond will break. The time interval between these two steps is very small and so $NO_2$ will also be produced quickly. These results are generally consistent with those obtained from classical reaction molecular dynamics.

**3.4. Reaction between RDX and HTPB.** The results of first-principles molecular dynamics calculations for the RDX/HTPB system were analyzed to examine the decomposition reactions of HTPB molecules. The outcome of this analysis is presented in Figure 8. The HTPB chains were found to primarily undergo dehydrogenation reactions as well as rupture of the carbon backbones. The low-molecular-weight products



https://doi.org/10.1021/acsomega.3c01160
ACS Omega 2023, 8, 18851−18862

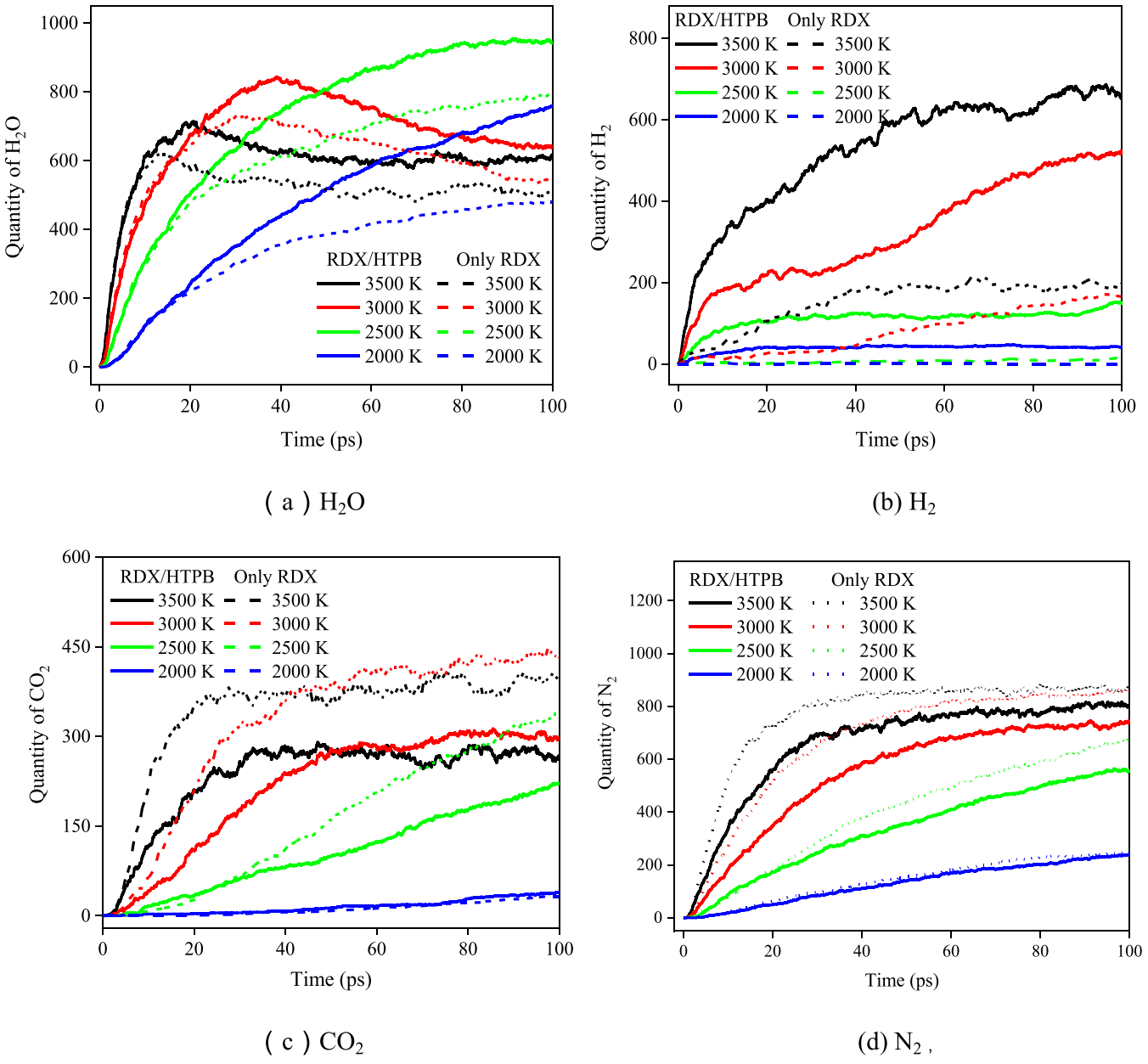


**Figure 11.** Quantities of the main decomposition products as functions of time for the RDX/HTPB and pure RDX systems at various temperatures.

obtained from such reactions could potentially react with the RDX decomposition products, thus affecting the end products from the decomposition of the mixed explosive.

Figure 9 summarizes the results of the first-principles calculations for the RDX/HTPB system at 3000 K. Several reactions, as presented here, were determined to occur between the small molecules generated by RDX decomposition and the decomposition products of the HTPB during the later stages of the decomposition process. In reaction 1, a H atom detaches from an HTPB chain at 0.45 ps and, at 0.47 ps, combines with the RDX decomposition product NO to form HNO as an intermediate. He et al.[17] also found that the O atoms in nitro groups in HMX decomposition products will readily bond with H atoms from HTPB to generate intermediates such as HONO, OH, and HNO, which may then be converted to $H_2O$, NO, and $NO_2$. In the case of reaction 2, $NO_2$ is released from an RDX molecule at 0.15 ps after which, at 0.16 ps, this molecule approaches an HTPB molecule. At 0.20 ps, the $NO_2$ reacts with the broken HTPB chain to form a new C−N bond. This same type of reaction was also evident in the classical molecular dynamics simulations.

**3.5. Main Thermal Decomposition Products.** The RDX/HTPB mixed system will generate a large number of low-molecular-weight products during thermal decomposition reactions. Figure 10 plots the amounts of the primary product $NO_2$ generated over time in both the RDX/HTPB and pure RDX systems. During the initial stage of the reaction, the N−$NO_2$ bonds in RDX molecules were initially broken to generate a large quantity of $NO_2$ and so the amount of this product increased rapidly. Subsequently, $NO_2$ participated in various secondary reactions and so the concentration of $NO_2$ decayed. In both systems, higher temperatures accelerated this decrease in the amount of $NO_2$. As can be seen from the expanded view



https://doi.org/10.1021/acsomega.3c01160
ACS Omega 2023, 8, 18851−18862

of the graph, the rate of increase was greater in the case of the pure RDX and the peak quantity was higher compared with the RDX/HTPB. These results can possibly be attributed to the reaction of a portion of the $NO_2$ with HTPB in the latter system.

Figure 11 plots the quantities of various final products obtained for the RDX/HTPB and pure RDX systems. As can be seen from the figure, significant amounts of $H_2O$, $H_2$, $CO_2$, and $N_2$ were generated. $N_2$ was obtained primarily from the conversion of $NO_2$ and NO based on secondary reactions. It is also apparent that the amount of $N_2$ eventually reached an equilibrium value. At all temperatures, the rate of increase in the amount of $N_2$ was higher in the pure RDX system as was the quantity at equilibrium. These results are ascribed to the reactions of carbon-chain fragments produced by HTPB decomposition with some $NO_2$ or NO in the RDX/HTPB system. In contrast, the quantities of $H_2O$ and $H_2$ were found to increase over time and the growth rates and equilibrium quantities of both products were greater in the case of the RDX/HTPB system. Previous studies have demonstrated that the HTPB alkyl groups in the RDX/HTPB system will undergo numerous dehydrogenation reactions, leading to the generation of more $H_2O$ and $H_2$ compared with pure RDX. The amount of $CO_2$ increased continuously until equilibrium, and higher temperatures increased the rate at which this product was obtained. Following ring opening of the RDX molecule, a variety of carbon-chain fragments were generated that eventually formed $CO_2$. Because the RDX/HTPB system contained many such chains, the generation of $CO_2$ was hindered and the growth rate was significantly lower than that for the pure RDX.

## 4. CONCLUSIONS

A classical reactive molecular dynamics method based on the ReaxFF-lg force field and a first-principles molecular dynamics method based on SCC-DFTB theory were used to simulate the thermal decomposition of an RDX/HTPB mixed explosive. Details of the reactions of both RDX and HTPB during the thermal decomposition process were analyzed. The effects of HTPB on the RDX thermal decomposition rate and on product formation were also examined. The results show that the presence of a small amount of HTPB will significantly reduce the RDX decomposition rate. During the initial stage of the reaction, $N-NO_2$ bonds are broken to generate $NO_2$ from the RDX/HTPB system at various temperatures, but lower temperatures promote hydrogen transfer reactions. After $N-NO_2$ bond breaking, the rupture of a C−N bond induces ring opening and this step competes with the breaking of a N−N bond. Under high-temperature conditions, HTPB primarily undergoes dehydrogenation and chain breaking. Free H will subsequently react with the RDX decomposition products, and the broken HTPB chains will also combine with $NO_2$. The reaction between HTPB and RDX leads to greater equilibrium quantities of the final products $H_2O$ and $H_2$ than are obtained from pure RDX but less $N_2$ and $CO_2$. The thermal decomposition reactions of the mixed explosive systems are evidently complicated, and so it is important to develop detailed reaction mechanisms to ensure the safe use and storage of these energetic materials.

## AUTHOR INFORMATION


### Corresponding Author

**Junying Wu** − *State Key Laboratory of Explosion Science and Technology, Beijing Institute of Technology, Beijing 100081, China*; orcid.org/0000-0002-9776-559X; Email: wjy1312@bit.edu.cn

### Authors

**Jiaojiao Wu** − *State Key Laboratory of Explosion Science and Technology, Beijing Institute of Technology, Beijing 100081, China*

**Junjian Li** − *State Key Laboratory of Explosion Science and Technology, Beijing Institute of Technology, Beijing 100081, China*

**Yiping Shang** − *State Key Laboratory of Explosion Science and Technology, Beijing Institute of Technology, Beijing 100081, China*

**Lang Chen** − *State Key Laboratory of Explosion Science and Technology, Beijing Institute of Technology, Beijing 100081, China*; orcid.org/0000-0003-2623-1061

Complete contact information is available at: https://pubs.acs.org/10.1021/acsomega.3c01160


### Notes

The authors declare no competing financial interest.

## ACKNOWLEDGMENTS

This work was supported by the National Natural Science Foundation of China (Grant 11832006).

## REFERENCES


(1) Wang, C.; Zhang, C.; Xue, X. Pressure and Polymorph Dependent Thermal Decomposition Mechanism of Molecular Materials: A Case of 1, 3, 5,-Trinitro-1, 3, 5,-triazine. *J. Phys. Chem. A* **2022**, *126*, 463−472.

(2) Ravaji, B.; Wilkerson, J. W. Effects of crystallography on hot-spot formation in porous RDX single crystals. *Extreme Mech. Lett.* **2021**, *42*, No. 101112.

(3) Raabe, D. *Computational Materials Science: The Simulation of Materials Microstructures and Properties*; Wiley-VCH Verlag GmbH, 1998.

(4) Wang, F.; Chen, L.; Geng, D.; Lu, J.; Wu, J. Effect of density on the thermal decomposition mechanism of ε-CL-20: a ReaxFF reactive molecular dynamics simulation study. *Phys. Chem. Chem. Phys.* **2018**, *20*, 22600−22609.

(5) Mei, Z.; An, Q.; Zhao, F. Q.; Xu, S. Y.; Ju, X. H. Reactive molecular dynamics simulation of thermal decomposition for nano-aluminized explosives[J]. *Phys. Chem. Chem. Phys.* **2018**, *20*, 29341−29350.

(6) She, C.; Jin, S.; Chen, S.; Li, L.; Shu, Q.; Chen, Y.; Wang, J.; Wu, N.; Chen, M.; Chen, K. Reactive molecular dynamics simulation of thermal decomposition for nano-FOX-7. *Appl. Phys. A: Mater. Sci. Process.* **2021**, *127*, No. 881.

(7) Strachan, A.; Kober, E. M.; Van Duin, A. C.; Oxgaard, J.; Goddard, W. A., III Thermal decomposition of RDX from reactive molecular dynamics. *J. Chem. Phys.* **2005**, *122*, No. 054502.

(8) Peng, L. J.; Yao, Q.; Wang, J. B.; Li, Z. R.; Zhu, Q.; Li, X. Y. Pyrolysis of RDX and its derivatives via reactive molecular dynamics simulations. *J. Chem. Phys.* **2017**, *33*, 745−754 (in Chinese).

(9) Chen, F.; Cheng, X. Thermal decomposition behaviour of hexahydro-1,3,5-trinitro-1,3,5-triazine (RDX) under shock velocities by molecular dynamics simulation. *J. At. Mol. Sci.* **2016**, *33*, 315−319.

(10) Gump, J. C.; Peiris, S. M. Comparison of Reaction Kinetics of I-RDX and RDX at High Pressure. *AIP Conf. Proc.* **2006**, *845*, 1069−1072.




https://doi.org/10.1021/acsomega.3c01160
*ACS Omega* 2023, 8, 18851−18862

(11) Feng, S.; Guo, F.; Yuan, C.; Cheng, X.; Wang, Y.; Zhang, H.; Chen, J.; Su, L. Effect of neutron irradiation on structure and decomposition of $\alpha$-RDX: A ReaxFF molecular dynamics study. *Comput. Theor. Chem.* **2023**, *1219*, No. 113965.
(12) Zhao, Y.; Zhao, F. Q.; Xu, S. Y.; Ju, X. H. Molecular reaction dynamics simulation of thermal decomposition for aluminiferous RDX composites. *Comput. Mater. Sci.* **2020**, *177*, No. 109556.
(13) Zhang, L.; Zybin, S. V.; Van Duin, A. C.; Dasgupta, S.; Goddard, W. A., III Thermal Decomposition of Energetic Materials by ReaxFF Reactive Molecular Dynamics. *AIP Conf. Proc.* **2006**, *845*, 589−592.
(14) Xu, J.; Zhao, J.; Sun, L. Thermal decomposition behaviour of RDX by first-principles molecular dynamics simulation. *Mol. Simul.* **2008**, *34*, 961−965.
(15) Guo, D.; An, Q.; Zybin, S. V.; Goddard, W. A., III; Huang, F.; Tang, B. The co-crystal of TNT/CL-20 leads to decreased sensitivity toward thermal decomposition from first principles based reactive molecular dynamics. *J. Mater. Chem. A* **2015**, *3*, 5409−5419.
(16) Manaa, M. R.; Fried, L. E.; Melius, C. F.; Elstner, M.; Frauenheim, T. Decomposition of HMX at extreme conditions: A molecular dynamics simulation. *J. Phys. Chem. A* **2002**, *106*, 9024−9029.
(17) He, Z. H.; Huang, Y. Y.; Ji, G. F.; Chen, J.; Wu, Q. Electron properties and thermal decomposition behaviors for HMX/HTPB plastic-bonded explosives. *J. Phys. Chem. C* **2019**, *123*, 23791−23799.
(18) Woińska, M.; Grabowsky, S.; Dominiak, P. M.; Woźniak, K.; Jayatilaka, D. Hydrogen atoms can be located accurately and precisely by x-ray crystallography. *Sci. Adv.* **2016**, *2*, No. e1600192.
(19) Martínez, L.; Andrade, R.; Birgin, E. G.; Martínez, J. M. PACKMOL: A package for building initial configurations for molecular dynamics simulations. *J. Comput. Chem.* **2009**, *30*, 2157−2164.
(20) CP2K Developer Group. *CP2K Home Page*. http://www.cp2k.org/.
(21) van Duin, A. C. T.; Dasgupta, S.; Lorant, F.; Goddard, W. A. ReaxFF: a reactive force field for hydrocarbons. *J. Phys. Chem. A* **2001**, *105*, 9396−9409.
(22) Liu, L.; Liu, Y.; Zybin, S. V.; Sun, H.; Goddard, W. A., III ReaxFF-lg: Correction of the ReaxFF reactive force field for London dispersion, with applications to the equations of state for energetic materials. *J. Phys. Chem. A* **2011**, *115*, 11016−11022.
(23) Fröhlich, M. G.; Sewell, T. D.; Thompson, D. L. Molecular dynamics simulations of shock waves in hydroxyl-terminated polybutadiene melts: mechanical and structural responses. *J. Phys. Chem. A* **2014**, *140*, No. 024902.
(24) Yang, Z.; He, Y. H. Pyrolysis of octanitrocubane via molecular dynamics simulations. *Acta Phys.-Chim. Sin.* **2016**, *32*, 921−928.


https://doi.org/10.1021/acsomega.3c01160
*ACS Omega* 2023, 8, 18851−18862